

Fatigue Crack Growth Rate, Microstructure and Mechanical Properties of Diverse Range of Aluminum Alloy: a Comparison

Abdessamad BRAHAMI
Benattou BOUCHOUICHA
Mokhtar ZEMRI

*Laboratoire de Matériau et des Systèmes Réactifs
Djilali Liabes University of Sidi Bel Abbes, Algeria
abdouda2002@gmail.com*

Jamal FAJOUJ
*Institut de Recherche Engénierie Civil et Mécanique
IUT de Saint-Nazaire GeM, France*

Received (13 October 2017)

Revised (25 October 2017)

Accepted (30 November 2017)

In practice for all metallic materials, damage by fatigue usually takes in two steps, the appearance of an initial crack which then grows as a function of the present microstructure. The objective of this study is to identify the elements influencing the fatigue crack growth rate on aluminum alloys of different microstructures. Characterization tests and microstructural analysis on 2024-T3, 5083-H22, 6082-T6 and 7075-T6 shades have been carried out. Based on the experimental results obtained, AA7075-T6 has the best fatigue crack rate resistance which is explained by its behavior as well as the nature and dispersive distribution of the secondary element.

Keywords: aluminum alloy, fatigue crack growth, mechanical properties, microstructure, precipitation.

1. Introduction

The mechanical strength of pure aluminum is relatively weak which prevents its use for some applications. The mechanical strength of aluminum can be remarkably increased by the addition of other elements, thus forming alloys [1-3].

To optimize the static properties and damage tolerance of aluminum, elements such as copper, zirconium, magnesium, lithium, manganese or even silver are added. During thermo-mechanical treatments, these added elements can form insoluble dispersants which play a key role in the control of recrystallization, or fine precipitates inducing structural hardening which increases the static properties of the metal [4-5].

One of the most important axes for optimizing the performance of these materials is mechanical fatigue characterization, which is the main cause for the occurrence of defects [8-9]. It is therefore necessary to take this fatigue phenomenon into account in order to guarantee the reliability and safety of a component right from the design stage. From the experimental point of view, the principle is to put the test specimens under specific and known conditions in order to determine the lifetime of the material. However, fatigue tests are time consuming and costly.

Several research studies have been conducted on the influence of the microstructure [10-11], the stress ratio [12] and the mean stress [13] on the fatigue crack growth rate of aluminum alloys.

In the present work, the various factors, the microstructure, the nature of precipitates and the mechanical properties influencing the fatigue behavior of the various aluminum alloys (2024-T6, 5083-H22, 6082-T6 et 7075-T6) are studied through mechanical characterization tests and microstructural analysis. A particular study on the influence of the nature and distribution of different precipitates of each shade on the crack growth rate has been carried out. These precipitates and their chemical compositions will be subsequently determined using firstly a Scanning Electron Microscope (SEM) and secondly the Energy Dispersive Spectroscopy (EDS).

2. Experimental procedure

This study is divided into two main parts: (1) a mechanical characterization based on tensile tests, microhardness and fatigue crack growth to correctly identify the laws of behavior governing the lifetime of the materials used, and (2) a microstructural analysis to locate and identify the precipitates of the different phases by EDS dispersive energy spectroscopy.

2.1. Materials

The materials used in this study are 2024-T3, 5083-H22, 6082-T6 and 7075-T6 aluminum alloys with a sheet thickness of 4 mm. Table 1 gives the chemical composition of these alloys as determined by EDS method.

Table 1 Typical chemical composition of the aluminum alloys (% weight)

Element (%)	fSi	Mg	Fe	Cu	Mn	Cr	Zn	Ti	Al
6082-T6	1,59	1,29	1.04	0,41	0.68	0,14	0,31	0,21	BAL.
7075-T6	0.51	2.71	0.23	1.65	0.29	0.31	4.48	0.22	BAL.
2024-T3	0.06	1.57	0.17	4.45	0.56	0.1	0.16	0.15	BAL.
5083-H22	0.57	1.38	0.64	0.42	1.19	0.05	0.01	0.04	BAL.

2.2. Testing procedure

2.2.1. Tensile test

Monotonic tensile tests were performed on an INSTRON 8516 testing machine to determine the mechanical properties of the materials. The tests were performed using

standard rectangular tension specimens according to ASTM E8 [14] with a moving crosshead speed set at 1 mm/min, at room temperature and in air-laboratory. The dimensions of the specimen are given in Figure 1.

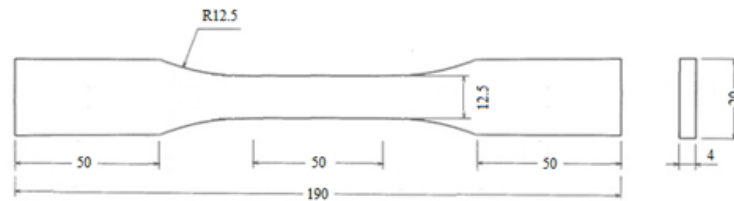


Figure 1 Tensile test specimen

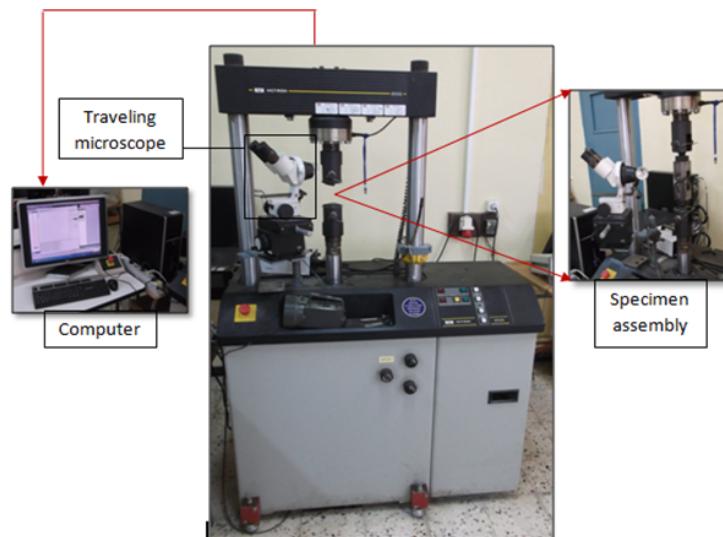


Figure 2 Computer controlled servo-hydraulic INSTRON 8516 testing machine

2.2.2. Microhardness test

The microhardness was measured using standard Vickers on a SHIMADZU HMV-2000 microhardness tester, using 1000 g load for 10 s. An average of five readings was recorded. The microhardness tests were performed on a 20 mm by 20 mm coupons.

2.2.3. Microstructure observation

All samples for microstructure observation were cut from different materials with a dimension of 10 mm by 10 mm. For microstructure observation, the samples

were polished by 1400 abrasive paper. Qunata 250 field emission scanning electron microscopy (FE-SEM) with an EDS was used to observe the evolution of the microstructure and to perform analysis in order to determine chemical composition for the materials and then identify the precipitates of each grade as well as its chemical composition.

2.2.4. Fatigue test

All fatigue experiments were carried out under constant load amplitude, at room temperature and on a computer controlled servo-hydraulic INSTRON 8516 testing machine presented in Figure 2, following the ASTM E647-00 standard [15].

Crack propagation was monitored through visual measurements using a travelling microscope. The 50 mm wide compact tension (CT) specimens were tested for a 20Hz load frequency. Figure 5 illustrates the geometry and dimensions of the tested specimens. The following equation was used to determine the stress intensity factor:

$$\Delta k = \frac{\Delta P}{B} \sqrt{\frac{\pi a}{2w} \sec \frac{\pi a}{2}} \quad (1)$$

where P is the load in MPa, B and w are the thickness and width of the sample in cm, respectively, a is the crack length; and $a = 2a/w$.

That is to say that the determination of the maximum load and load ratio of each material used in the fatigue tests are determined beforehand.

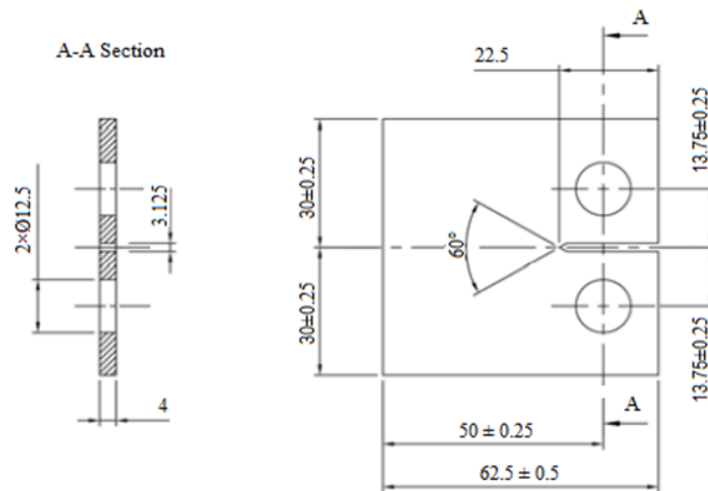


Figure 3 Compact tension specimen

3. Experimental procedure

3.1. Tensile test

A typical engineering stress-strain curve of the different aluminum alloy is presented in Figure 4, from which the mechanical characteristic are illustrated in Table 2. Obviously, the 7075-T6 aluminum alloy have the highest strength of about 587 MPa compared to the other alloy, and the uniform elongation close to 0.023%. The above results reveal that the 5083-H22 aluminum alloy has the lowest mechanical characteristic.

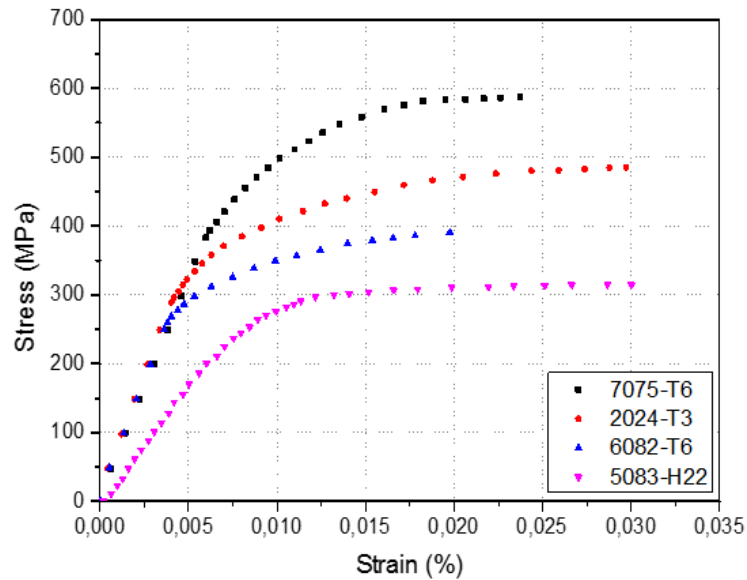


Figure 4 Tensile properties for all material

Table 2 Tensile strength properties of different aluminum alloys

Materials	E(Mpa)	R_e (MPa)	R_m (MPa)	K (MPa)	n
AA 7075-T6	66000	383	587	924	0.17
AA 2024-T3	74000	314	487	1351	0.21
AA 6082-T6	69000	260	391	848	0.19
AA 5083-H22	60000	190	317	578	0.15

The difference noted between the three grades (7075-T6, 2024-T3 and 6082-T6) on the one hand and the 5083-H22 grade on the other hand is explained by the fact that the first three belong to the second group representing the alloys whose mechanical

properties are determined by the heat treatment or structural hardening, generally carried out at the end of the transformation process. The hardening phenomenon results from the induced and controlled precipitation of certain phases inside the aluminum matrix which will produce an increase in mechanical properties. On the other hand, grade 5083-H22 belongs to the first group of hardening-hardening alloys whose mechanical properties are determined by the plastic hardening which corresponds to a structural modification of the metal, which is therefore weaker.

3.2. Microhardness test

Lists may be laid out with each item marked by a dot: The measurement of the Vickers microhardness for the different grades of aluminum alloy is presented in the following table:

Table 3 Vickers hardness of the materials

Material	2024-T3	5083-H22	6082-T6	7075-T6
Hardness [Hv]	102	111	109	184

The hardness of the heat treatment aluminum alloys, namely 2024-T3 and 6082-T6, is lower than the strain hardening alloys 5083-H22, due to the structural change by plastic hardening to the latter. The hardness of 7075-T6 is higher than that of 2024-T3 because of the precipitates of magnesium and zinc formed during alloying, while in 2024-T3 the precipitates of copper and magnesium are less important in terms of hardness.

3.3. Fatigue crack growth

The experimental fatigue crack growth rate (da/dN) versus stress intensity factor range (ΔK) data was derived using the seven point polynomial incremental technique [15]. The experimental data was correlated using the Paris law [16]. Figure 5 illustrates the crack propagation data derived for the 7075-T6, 6082-T6, 5083-H22 and 2024-T3 aluminum alloy. The Paris law was fitted with high correlation coefficient. For all materials, the stress ratio tested was $R = 0.1$.

The curves have a nearly a straight line shape over a large part of the area explored, which may be presented by the law of Paris of the form [17]:

$$\frac{da}{dN} = C (\Delta k)^m \quad (2)$$

where C and m are the parameters of the material. The results of the fatigue tests obtained for the four materials are summarized in Table 4.

For the same level of ΔK ($8 \text{ MPam}^{1/2}$), the crack growth rate of the alloy 5083-H22 is slightly higher than that of the alloy 6082-T6. However, a very large difference is recorded between these two alloys and that of 2024-T3. This difference gives the latter a very high resistance relative to the first two. This phenomenon can be explained by the dominant additive element in AA2024 (copper) which has a very high hot strength and high endurance. The AA7075-T6 alloy has a better resistance than that of 2024-T3, which is justified by the presence of zinc in addition

Table 4 Equations characterizing the Paris Law for the different materials

Mterials	Paris Law	ΔK
7075-T3	$da/dN=1,7E^{-7} \Delta K^{2,55}$	11 à 38 MPa \sqrt{m}
2024-T3	$da/dN= 5,35E^{-8} \Delta K^{3,23}$	7 à 18 MPa \sqrt{m}
6082-T6	$da/dN=1,9E^{-6} \Delta K^{2,44}$	5 à 12 MPa \sqrt{m}
5083 H22	$da/dN=1,29E^{-6} \Delta K^{2,53}$	3.5 à 8 MPa \sqrt{m}

to copper, which by its malleability and its electrical and thermal conductivity has a mechanical characteristic close to ferrous metals.

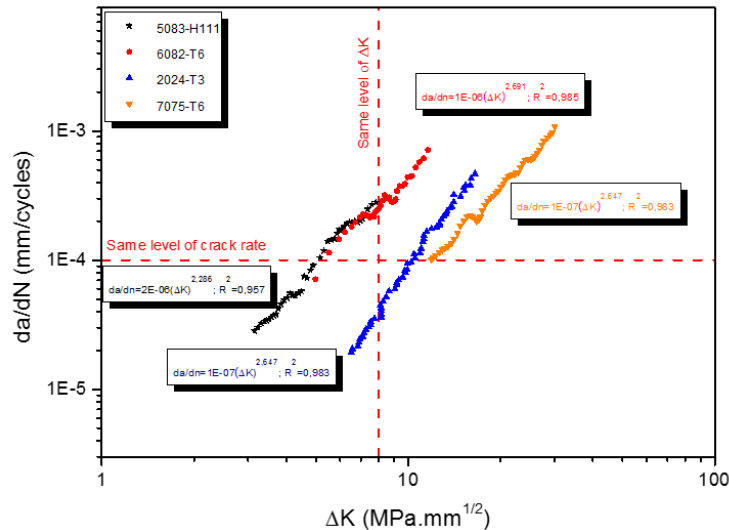


Figure 5 Log-log plot of da/dN versus ΔK for all materials

And for the same level of da/dN ($1E-4$), the two alloys 5083-H22 and 6082-T6 have practically the same level of ΔK . But this level is doubled in comparison to that of the alloy AA2024-T3, which characterizes the ductile aspect for the latter.

3.4. MEB observation

The results of the mechanical characterization tests obtained are confirmed by the microscopic analysis of the truncated and polished samples using a SEM.

After qualitative analysis on the 5083-H22 alloy, Figure 6 (d) shows the presence of the two elements Al and Mg to the exclusion of any other element detectable at the sensitivity threshold of the method.

Point analyzes of the zones of different contrasts: The impurity elements which give the course of solidification of Al_3Mg_2 compounds near the grain boundary.

These compounds do not improve the fatigue strength due to their breaks and their decohesions with the matrix, providing a low resistance level when the local deformation exceeds a critical value. These results can be compared with the data recorded on the phase diagram of the alloy, which demonstrates that the results are very realistic.

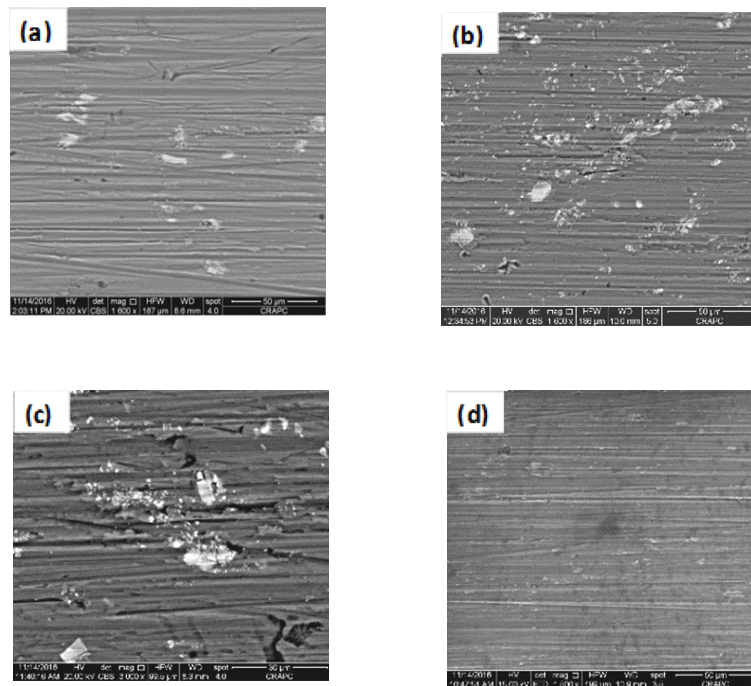


Figure 6 MEB observation for : a) AA5083-H111, b) AA6082-T6, c) AA2024-T3, d) AA7075-T6

On the other hand, a quantitative analysis point by point on samples 7075 and 2024 highlights, qualitatively, a phenomenon of Zinc diffusion in the copper for the first and the manganese in the copper for the second. There is also a constant composition within the domains with an inclined interface, giving rise to the two phases $MgZn_2$ for the first and Al_2CuMg for the second, which explains the higher level of resistance.

In order to clarify the results discussed above, the following figure describes the point analysis by the EDS method localizing each type of precipitate, in order to identify them and determine their chemical composition. The precipitate of each shade is marked with a yellow circle in the SEM image of Fig. 6.

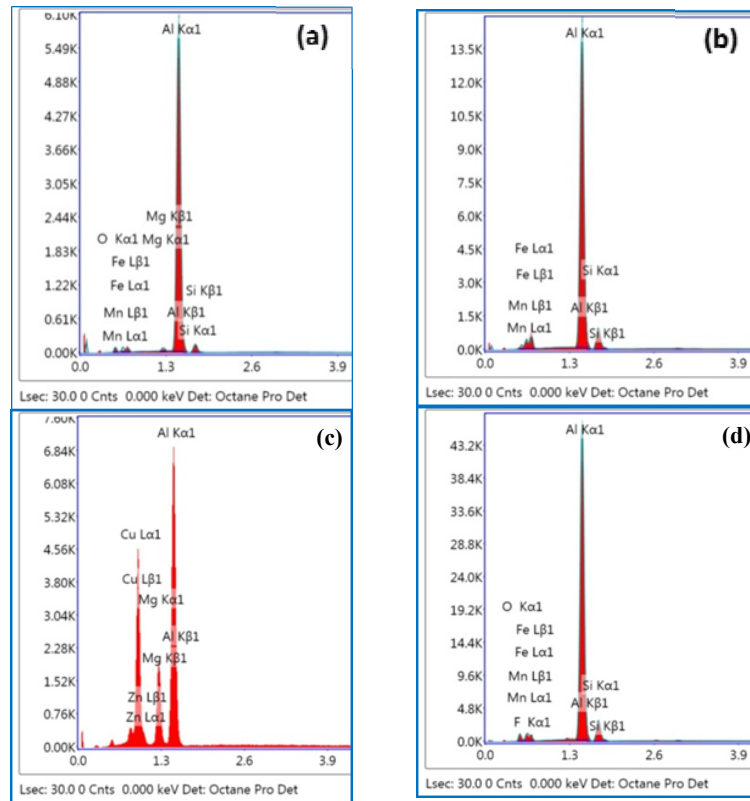


Figure 7 EDS analyze for: a) AA6082-T6, b), AA2024-T3 c) AA7075-T6, d) AA5083-H22

4. Conclusion

This study focused on the influence of the microstructure of different grades of aluminum alloy on the mechanical properties and the fatigue behavior of these alloys. The main characterization tests used are tensile tests, microhardness measurements and fatigue crack rate resistance. The different alloys studied have different percentage of additive elements, thus avoiding differences in mechanical behavior. The main conclusions drawn from the study are:

1. The elastic limit of the heat treatment alloys is higher than the strain hardening alloys.
2. The fatigue crack growth rate is remarkably low for the 6082-T6 and 5083-H22 alloys than for the 2024-T3 and 7075-T6 alloys for: On the one hand, the non-dispersive distribution of the secondary element of the first two alloys and dispersing for the others makes the latter more resistant. Also, the presence of silicon (Si) and manganese (Mn) in the first two alloys weakens fatigue resistance, whereas magnesium and copper generate more resistant precipitates.

3. Ductility, characterized by elongation, plays a primary role in fatigue resistance for different shades; the more ductile they are the more resistant they are.

In summary, the fatigue resistance is influenced by several factors not only the microstructure and mechanical properties but also the nature and distribution of the element of the secondary phase which has a high sensitivity to the addition elements.

Acknowledgements

The authors would like to acknowledge the advanced development and technology center (CDTA) and the center for scientific and technical research in physico-chemical analysis (CRAPC) for their helping in the experimental activities. Special thanks should also be given due to Dr. Mouloud DENAI for his support.

References

- [1] **Rana, R. S. and al.:** Reviews on the influences of alloying elements on the microstructure and mechanical properties of aluminum alloys and aluminum alloy composites, *International Journal of Scientific and Research Publications*, 2, 6, **2012**.
- [2] **Medrano-Prietoa, H. M. and al.:** Evolution of Microstructure in Al-Si-Cu System Modified with a Transition Element Addition and its Effect on Hardness, *Mat. Res.*, 19, 1, **2016**.
- [3] **Zhang, X. and al.:** Influence of Alloying Element Addition on Cu–Al–Ni High-Temperature Shape Memory Alloy without Second Phase Formation, *Acta Metallurgica Sinica*, 29, 9, **2016**.
- [4] **Samuel, A. M. and al.:** Role of Zr and Sc addition in controlling the microstructure and tensile properties of aluminum–copper based alloys, *Materials and Design*, 88, 1134–1144, **2015**.
- [5] **Shen, F. and al.:** Effects of secondary particle-induced recrystallization on fatigue crack growth in AA2524/AlCuMg T3 alloy sheets, *Journal of Alloys and Compounds*, 685, 571–580, **2016**.
- [6] **Anderson, T. L.:** Fracture Mechanics: Fundamentals and Applications, 3rd ed. *CRC Press, Boca Raton*, **2004**.
- [7] **Sih, G. C., Wei, R. P. Erdogan, F.:** Linear Fracture Mechanics: Historical Developments and Applications of Linear Fracture Mechanics, *Lehigh University Envo Publisher, Pennsylvania*, **1975**.
- [8] **Li, M. and al.:** Microstructure dependent fatigue crack growth in Al–Mg–Sc alloy, *Materials Science & Engineering*, 142–151, **2014**.
- [9] **Sun, Y. P., Yan, H. G., Chen, Z. H.:** Microstructure and mechanical properties of Al–Zn–Mg–Cu/SiC composite after heat treatment, *Met Sci Heat Treat*, 51, 394, **2009**.
- [10] **Tang, K. K.:** Fatigue crack growth in the micro to large scale of 7075-T6 Al sheets at different R ratios, *Theoretical and Applied Fracture Mechanics*, 83, 93–104, **2016**.
- [11] **Maddox, S. J.:** The effect of mean stress on fatigue crack propagation a literature review, *international Journal of Fracture*, 11, 3:389-408, **1975**.
- [12] ASTM Standard E8-04: Standard Test Methods for Tension Testing of Metallic Materials, Part 03.01, *Metals Mechanical Testing Elevated and Low-Temperature Tests Metallographic*.

- [13] ASTM Standard E647-00: Standard Test Method for Measurement of Fatigue Crack Growth, *Part 03.01, Metals Mechanical Testing Elevated and Low-Temperature Tests Metallographic*.
- [14] **Paris, P. C., Erdogan, F.:** A critical analysis of crack propagation laws, Transactions of The ASME, *Series E: Journal of Basic Engineering*, 85, 528–534, **1963**.

